Inhibitor Discovery Targeting the Intermediate Structure of β-Amyloid Peptide on the Conformational Transition Pathway: Implications in the Aggregation Mechanism of β-Amyloid Peptide†

Dongxiang Liu,*,‡ Yechun Xu,‡ Yu Feng,‡ Hong Liu,‡ Xu Shen,‡,§ Kaixian Chen,‡ Jianpeng Ma,||,⊥ and Hualiang Jiang*,‡,§

Center for Drug Design and Discovery, State Key Laboratory of Drug Research, Shanghai Institute of Materia Medica, Chinese Academy of Sciences, Shanghai 201203, China, School of Pharmacy, East China University of Science and Technology, Shanghai 200237, China, Department of Biochemistry and Molecular Biology, Baylor College of Medicine, One Baylor Plaza, BCM-125, Houston, Texas 77030, and Department of Bioengineering, Rice University, Houston, Texas 77005

Received May 14, 2006; Revised Manuscript Received July 5, 2006

ABSTRACT: Aβ peptides cleaved from the amyloid precursor protein are the main components of senile plaques in Alzheimer's disease. Aβ peptides adopt a conformation mixture of random coil, β-sheet, and α-helix in solution, which makes it difficult to design inhibitors based on the 3D structures of Aβ peptides. By targeting the *C*-terminal β-sheet region of an Aβ intermediate structure extracted from molecular dynamics simulations of Aβ conformational transition, a new inhibitor that abolishes Aβ fibrillation was discovered using virtual screening in conjunction with thioflavin T fluorescence assay and atomic force microscopy determination. Circular dichroism spectroscopy demonstrated that the binding of the inhibitor increased the β-sheet content of Aβ peptides either by stabilizing the *C*-terminal β-sheet conformation or by inducing the intermolecular β-sheet formation. It was proposed that the inhibitor prevented fibrillation by blocking interstrand hydrogen bond formation of the pleated β-sheet structure commonly found in amyloid fibrils. The study not only provided a strategy for inhibitor design based on the flexible structures of amyloid peptides but also revealed some clues to understanding the molecular events involved in Aβ aggregation.

Alzheimer's disease (AD[1]) is a progressive neurodegenerative disease that is characterized by extracellular amyloid plaques and intraneuronal fibrillary tangles in the brain (*1*−*3*). $A\beta_{1-40}$ and $A\beta_{1-42}$ are the main alloforms of amyloid β (Aβ) peptides found in amyloid plaques. Though the amount of secreted $A\beta_{1-42}$ is only 10% of $A\beta_{1-40}$, $A\beta_{1-42}$ is the predominant component in AD plaques (*4*, *5*) and displays an enhanced neurotoxicity relative to that of $A\beta_{1-40}$ (*6*, *7*). A number of mechanisms have been proposed to explain the neuron toxicity of Aβ peptides, including the formation of ion-channels on the cell membrane (*8*), the generation of free radicals (*9*−*11*), and the interaction of Aβ peptides with various receptors, such as apolipoprotein E (*12*−*14*) and mitochondrial hydroxyacyl-CoA dehydrogenase (*15*, *16*). The cytotoxic mechanism of Aβ has not been fully understood. However, compelling evidence indicates that the soluble oligomers (amyloid-derived diffusible ligands, ADDLs) and fibrils of Aβ are the toxic identities that cause neuronal injury and death in AD (*17*). Therefore, chemicals to prevent the pathological oligomerization and fibrillation of Aβ have potential therapeutic applications in the treatment of AD (*18*).

The *C*-terminal 12−14 amino acids of Aβ may exist as a helix in the cell membrane; however, the cleavage of Aβ from amyloid precursor protein (APP) by peptide bond hydrolysis could disrupt the helical conformation. The *N*-terminus of Aβ is outside the cell membrane, and its structure remains unknown. Therefore, the conformational transition of Aβ from α-helix to β-sheet or from random coil to β-sheet may occur during fibril formation *in vivo*. Aβ may adopt multiple conformations *in vitro*, such as α-helix, β-sheet, or random coil, depending on buffer conditions, such as pH, ion strength, and solvent properties.

† This work was supported by State Key Program of Basic Research of China (Grant 2004CB518901), "Introducing Outstanding Oversea Scientists Project" of Chinese Academy of Sciences (CAS), Basic Research Project for Talent Research Group from Shanghai Science and Technology Commission (SSTC), Shanghai Pu-Jiang Project (05PJ14110), Key Project from SSTC (Grant 02DJ14006), Key Project for New Drug Research from CAS and the Welch Foundation (Q-1512) granted to J.M.

* To whom correspondence should be addressed. Phone: 86-21-50806600. Fax: 86-21-50806065. E-mail: hljiang@mail.shcnc.ac.cn (H.J.); dxl@mail.shcnc.ac.cn (D.L.).

‡ Chinese Academy of Sciences.

§ East China University of Science and Technology.

|| Baylor College of Medicine.

⊥ Rice University.

[1] Abbreviations: AD, Alzheimer's disease; Aβ, β-amyloid peptide; APP, amyloid precursor protein; ADDLs, amyloid-derived diffusible ligands; BBB, blood−brain barrier; SMON, subacute myelo-optico-neuropathy; TFE, trifluoroethanol; HFIP, hexfluoro 2-propanol; DMSO, dimethyl sulfoxide; PBS, phosphate-buffered saline; Hmb, 2-hydroxy-4-methoxybenzyl; SDS, sodium dodecyl sulfate; ThT, thioflavin T; GTA, glutaraldehyde; MD, molecular dynamics; SBDD, structure-based drug design; CD, circular dichroism; AFM, atomic force microscope; TEM, transmission electron microscope; EM, electron microscope; NMR, nuclear magnetic resonance; QLS, quasielastic light scattering; CHO, Chinese hamster ovary; PICUP, photoinduced cross-linking of unmodified proteins.

10.1021/bi060955f CCC: $33.50
Published on Web 08/17/2006

For example, Aβ exists as a conformation mixture of α-helix, β-sheet, and random coil in aqueous solution (*19*, *20*). In fluorinated alcohols such as trifluoroethanol (TFE) or hexfluoro 2-propanol (HFIP), Aβ adopts an α-helical conformation (*21*−*24*). The pH and temperature also affect Aβ peptide conformation. The α-helical conformation of Aβ is favored at pH 1−4 and 7−10. The increase in temperature unfolds the helical conformation. On the contrary, the β-sheet conformation of Aβ is temperature insensitive and favored at pH 4−7 (*25*−*27*). X-ray diffraction analyses and NMR determinations revealed that the Aβ stack in the form of pleated β-sheet structures oriented perpendicular to the fibril axis (*28*−*30*). Conformational studies on Aβ fibrillogenesis by circular dichroism (CD) spectroscopy, quasielastic light scattering (QLS), and other kinetic methods suggested that the conformational transition of Aβ into β-sheet structure in fibrils goes through an α-helix-containing intermediate conformation (*31*−*33*). The structural complexity of Aβ makes it extraordinarily difficult to design new inhibitors based on the 3D structures of the peptides.

Thus far, several classes of chemical compounds have been reported to block the fibrillation of Aβ, such as antibiotics (*34*), benzofuran derivatives (*35*), sulfonated dyes (*36*, *37*), styryl benzene (*38*), flavone (*39*), and peptidic β-sheet breakers (*40*). Cell culture experiments demonstrated that inhibitors could reduce the cytotoxicity of Aβ peptides. The administration of Aβ inhibitors also reduced the amount of amyloid deposition in mice with acute amyloidosis (*41*). Even though, very few Aβ inhibitors have entered into clinic trial phases (*42*, *43*), the problems inherent with these inhibitors, such as low bioavailability, poor biostability, toxicity, and inability across the blood−brain barrier (BBB), have limited their therapeutic applications. For example, an experimental drug, clioquinol, found to dissolve amyloid plaques and possibly help relieve AD symptoms, is now in phase II clinical trials. However, this drug caused a tragic disease called subacute myelo-optico-neuropathy (SMON) in patients. It has been banned since 1970 in Japan (*44*, *45*). Accordingly, the structural modification of inhibitors as well as the design of new inhibitors with alternative structural scaffolds is required to improve physiochemical properties.

Previously, we had studied the conformation transition of Aβ_{1-40} from an α-helix to a random coil by using long time molecular dynamics (MD) simulations (*46*). The result revealed that Aβ undergoes an α-helix/β-sheet intermediate structure during the conformational transition. The α-helix/β-sheet intermediate structure has a core domain constituted by the segment of residues 24−37, of which four residues Gly25, Gly29, Gly33, and Gly37 are essential to β-sheet formation and amyloid fibrillation. Chemical compounds that lock the structure of Aβ into the α-helix/β-sheet intermediate state could possibly inhibit Aβ fibrillation. Accordingly, virtual screening based on molecular docking was performed, targeting the Aβ intermediate structure. In stead of stabilizing the α-helix conformation of nonaggregative Aβ intermediate structures, we aimed to design inhibitors binding to the β-sheet region of the Aβ intermediate to interrupt the formation of the pleated β-sheet structure found in amyloid fibrils. The aggregation and fibrillation of Aβ in the presence of one found inhibitor, DC-AB1, was studied by thioflavin T (ThT) fluorescence assay, atomic force microscopy (AFM), and polyacrylamide gel electrophoresis analysis, all of which showed that the inhibitor may effectively inhibit Aβ to form fibrils. Meanwhile, CD spectroscopy revealed that the β-sheet component of Aβ increased in the presence of DC-AB1, suggesting that DC-AB1 bound to Aβ and stabilized its β-sheet conformation. Taken together, this study not only demonstrated that the β-sheet region of Aβ intermediate structures could be used as a binding site for inhibitor design but also provided new insights into the molecular events involved in the conformational transition of Aβ peptides in fibrillogenesis.

EXPERIMENTAL PROCEDURES

Virtual Screening A stable conformation of Aβ_{1-40} that contained an α-helix and a β-sheet local structures was extracted from the trajectory of a 50-ns MD simulation on Aβ_{1-40} (*46*). The peptide surface mainly constituted of *C*-terminal residues Phe19, Phe20, Val24, Gly25, Gly29, Ala30, Gly33, Leu34, Gly38, Val39, and Val40 and a few *N*-terminal residues Ala2, Glu3, Arg5, Tyr10 was taken as the binding site for inhibitor design. Spheres were generated by the AutoMS and sphgen programs encoded in DOCK4.0 (*47*, *48*) (http://dock.compbio.ucsf.edu/) to describe the shape of the binding site. The hydrophobic and electrostatic properties of the binding site were calculated by the program Grid4. Molecules from the SPECS database (http://www.specs.net/) were docked into the binding site by using a parallelized DOCK4.0 on a PC cluster. Kollman-all-atom charges and Geisterger−Hückel charges were assigned to Aβ_{1-40} residues and small molecules, respectively. The conformational flexibility of small molecules was considered during the docking calculation. After the initial orientation, a grid-based rigid body minimization was carried out on small molecules to locate the nearest local energy minimum within the binding site. The position and conformation of each docked molecule were optimized using the single anchor search and torsion minimization method encoded in DOCK4.0. Twenty-five configurations per ligand and 50 maximum anchor orientations were used for the anchor-first search. All docked configurations were energy minimized with a cycle of 60 maximum iterations. The binding pose (oritention and conformation) of a small molecule on Aβ was examined with a scoring function approximating the ligand−receptor binding energy, which is the sum of van der Waals and electrostatic interaction energies. The top 1000 molecules ranked by DOCK were re-evaluated by Cscore (*49*) and inspected using the software Sybyl6.8 (Tripos, Inc., St. Louis, MO). Molecules with irrational interaction with Aβ_{1-40} were discarded from the list. The selected compounds were purchased from the SPECS company.

Preparation of Sample Solution. Aβ_{1-42} (Sigma-Aldrich, catalog no. A9810) was dissolved in dimethyl sulfoxide (DMSO) to make a 200 μM stock solution. Aβ_{1-40} (Sigma-Aldrich, catalog no. A4473) was dissolved in Millipore water to make a 1.5 mg/mL stock solution. Aβ_{1-42} and Aβ_{1-40} stock solutions were centrifuged at the speed of 12 000 rpm for 10 min. The above supernatant was used for experiments. Compounds purchased from SPECS were dissolved in DMSO at a concentration of 10 mM.

ThT Fluorescence Assay. A screening assay for compounds to inhibit Aβ fibrillation was performed by measuring ThT

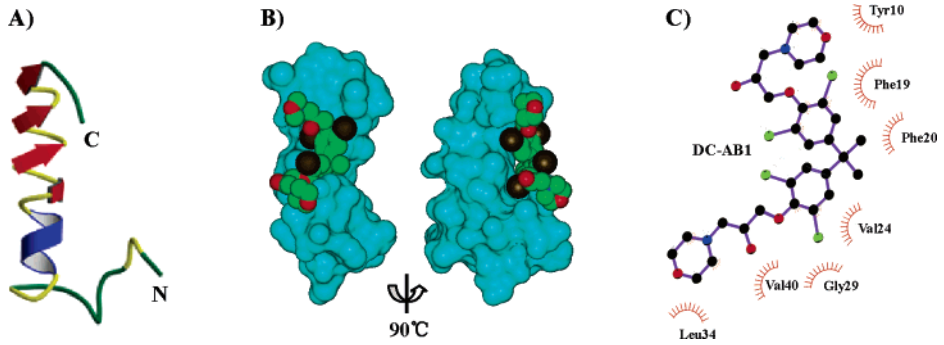

FIGURE 1: (A) Conformational transition intermediate structure of $A\beta_{1-40}$ used for virtual screening. The β-sheet region at the *C*-terminus is the binding site. (B) Complex model of DC-AB1 with $A\beta_{1-40}$ generated by the docking simulation. $A\beta_{1-40}$ is colored in cyan. (C) Interaction details of DC-AB1 with $A\beta_{1-40}$ according to the complex model. DC-AB1 binds to the *C*-terminal β-sheet region mainly through hydrophobic interactions. There are three major hydrophobic sites at the $A\beta_{1-40}$ peptide surface that hold the hydrophobic chemical groups of DC-AB1. Two phenyl rings of DC-AB1 interact with the hydrophobic sites constituted of the residues of Val24, Gly29, and Val40 or the residues of Tyr10, Phe19, and Phe20, respectively. The morpholine group of DC-AB1 interacts with the hydrophobic residues of Leu34 and Val40.

fluorescence emission with a modified procedure described by Lee et al. (*50*). Each compound (in concentrations of 0.1−10.0 mM) (2 μL) and 2 μL of 200 μM $A\beta_{1-42}$ were added into 76 μL of phosphate-buffered saline (PBS at pH 7.4) in a 96-well plate. After incubation for 1 h at room temperature, 80 μL of 5 μM ThT solution (in 50 mM glycine-NaOH at pH 8.5) was added to the reaction solution. Fluorescence emission was measured at 488 nm with an excitation wavelength of 430 nm on a multilevel HTS counter (TECAN, Genios Pro).

Inhibition of $A\beta_{1-42}$ Fibril Growth. $A\beta_{1-42}$ (2.5 μL) (200 μM) was mixed with different volumes (i.e., 0, 10, 20, 30, 40 μL) of 10 mM compound. PBS buffer was added to make the final volume 50 μL. Samples were incubated at 37 °C for 20 h followed by the addition of 100 μL of 7.5 μM ThT (in PBS at pH 7.4). Fluorescence emission was measured at 483 nm with an excitation wavelength of 430 nm on a Hitachi F-2500 fluorescence spectrophotometer (Hitachi High-Tech Corp., Japan).

Atomic Force Microscopy. The compound (2.5 μL) (10 mM) and 2.5 μL of 200 μM $A\beta_{1-42}$ were added to 45 μL of PBS buffer (20% TFE at pH 7.4). As a control, 2.5 μL of 200 μM $A\beta_{1-42}$ was added to 47.5 μL of PBS buffer (20% TFE at pH 7.4). Samples were incubated at 37 °C for 6 days, and a 3 μL sample solution was deposited on freshly cleaved mica and incubated for 5 min, then blown dry. The 7TESP tips used for the scan had a resonance frequency of 280−290 kHz. The scan rate varied from 1 to 3 Hz. Image data were acquired using the tapping mode on a Multimode Nano IIIa atomic force microscope (Veeco, Woodbury, NY).

Glutaraldehyde Cross-Linking. The sample was incubated with 42 mM glutaraldehyde (GTA) at room temperature for 20 min, followed by the addition of equal volumes of the polyacrylamide gel electrophoresis sample buffer to stop the reaction.

Gel Electrophoresis. $A\beta_{1-42}$ (3 μL) (200 μM) was incubated with or without 3 μL of 10 mM compound in a final volume of 20 μL in PBS buffer (20% TFE at pH 7.4) at 37 °C for 6 days. Then, 5 μL of the incubated $A\beta_{1-42}$ samples and the unincubated 30 μM $A\beta_{1-42}$ were cross-linked with glutaraldehyde. The uncross-linked $A\beta_{1-42}$ samples were analyzed with 10% native gel. The cross-linked and uncross-linked $A\beta_{1-42}$ samples were analyzed with 10% SDS−PAGE. Both gels were run in a Tris/Glycine system and developed by the silver-stain method.

CD Spectroscopy. The compound was dissolved in Millipore water to make a 54.7 μM solution. The samples prepared for the CD experiment were (1) 20 μM $A\beta_{1-40}$ with or without equimolar concentration of compound and (2) 20 μM $A\beta_{1-40}$ in 20% TFE with or without equimolar concentration of compound. CD spectra were recorded in a 0.1 cm path-length cuvette on a Jasco J-810 spectropolarimeter (JASCO Corporation, Japan). The data were the average of four times scans over a wavelength of 190−260 nm at room temperature. The background signal from water was subtracted. Deconvolution of CD spectra was performed with the software CDNN (*51*).

RESULTS

Candidate Compound Selection. By molecular dynamics simulation, we found that $A\beta_{1-40}$ goes through α-helix/β-sheet intermediate structures during the α-helix to random coil conformational transition (*46*). The *C*-terminus of $A\beta_{1-40}$ intermediates adopted a β-sheet conformation (Figure 1A). Virtual screening was performed targeting the *C*-terminal region. Using energy score as the preliminary method to evaluate the binding affinity of compounds with the target, 1000 compounds with an energy score of −32.91 to −57.58 kJ/mol were selected by the program DOCK4.0 from over 278 000 molecular identities in the SPECS database (version 2004). The binding affinity of selected compounds was re-evaluated with Cscore. Meanwhile, the interaction of compounds with $A\beta_{1-40}$ was visually inspected using the software Sybyl6.8. Compounds with an unfavorable interaction with $A\beta_{1-40}$ were excluded from the candidate list. Hit compounds in the final list had Cscore values of 4−5. As a result, 125 compounds were chosen for biological assay.

Identification of the Inhibitor DC-AB1. ThT exhibits a characteristic fluorescence spectral change upon binding to amyloid fibrils. The maximum emission wavelength was shifted from 445 to 482 nm (*52*). The more fibrils it binds, the stronger the fluorescence intensity will be. To perform high-throughput screening on candidate compounds for inhibitory activity against Aβ fibrillation, we measured the fluorescence emission of ThT at 488 nm with an incident light of 430 nm in $A\beta_{1-42}$ incubated with 10 mM test

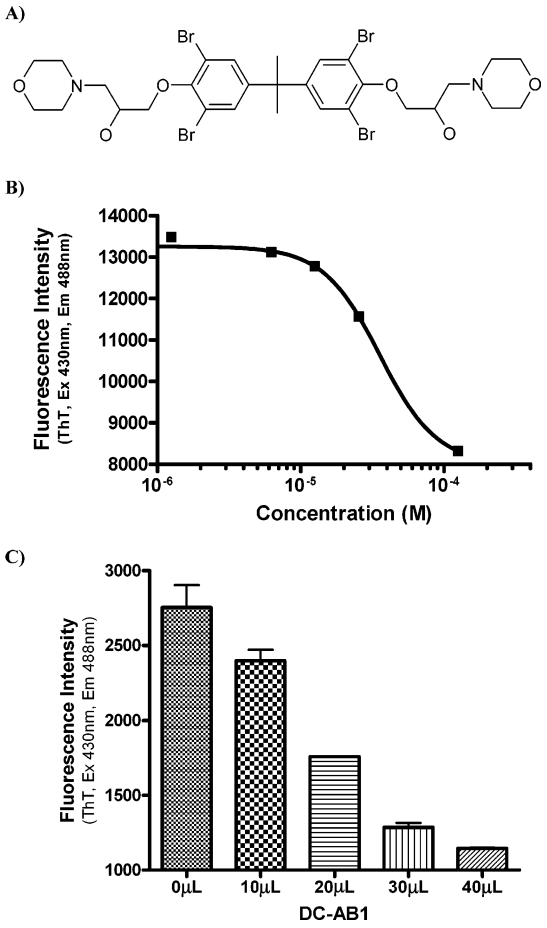

FIGURE 2: (A) Chemical structure of DC-AB1. (B) Concentration-dependent inhibition of DC-AB1 against Aβ fibrillation. (C) Amount of Aβ_{1-42} fibrils formed after 20 h of incubation at 37 °C. Aβ_{1-42} (2.5 μL of 200 μM) are incubated with 0, 10, 20, 30, and 40 μL of 10 mM DC-AB1, respectively. The decrease in fluorescence emission indicates the reduced amount of Aβ_{1-42} fibrils formed, proving the inhibitory activity of DC-AB1.

compounds. The ThT fluorescence from Aβ_{1-42} incubated without candidate compounds was taken as the control. In case of possible fluorescence emission from the compound, the fluorescence emitted from ThT with 10 mM compound was subtracted as the background. If a compound was found to reduce Aβ_{1-42} fibril formation at 10 mM, we performed further assays at several concentrations to confirm inhibitory activity. Of the 125 candidate compounds selected from virtual screening, one compound, designated DC-AB1, potently inhibits Aβ_{1-42} fibrillation in a concentration-dependent manner (Figure 2B). DC-AB1 has no absorption at the excitation wavelength (data not shown) and, therefore, does not interfere with the ThT fluorescence assay. The concentration of DC-AB1 needed to abolish half the amount of 2.5 μM Aβ_{1-42} fibril formation is 35.6 μM. According to the docking calculation, DC-AB1 has an energy score of −38.71 kJ/mol and a Cscore value of 4.

The inhibitory activity of DC-AB1 can also be demonstrated by measuring the amount of Aβ_{1-42} fibrils formed after 20 h of incubation with the presence of DC-AB1 at 37 °C. As shown in Figure 2C, the fluorescence intensity from ThT in Aβ_{1-42} incubated without DC-AB1 was about 2700 RFU. As the concentration of DC-AB1 was increased, the fluorescence emission decreased to about 1100 RFU, suggesting that less Aβ_{1-42} fibrils had formed. The reduction of Aβ_{1-42} fibrils shown in Figure 2C also proved the concentration-dependent inhibition of DC-AB1.

Effect of DC-AB1 on the Ultrastructure of Aβ Oligomers and Fibrils. It has been shown that Aβ_{1-42} can form fibrils in 20% TFE, even at nanomolar concentration (*22*). Thus, we incubated 10 μM Aβ_{1-42} in PBS buffer (20% TFE at pH 7.4) to study Aβ fibrillation by atomic force microscopy. After 6 days of incubation at 37 °C, Aβ_{1-42} aggregated into spheroidic species, where protofibrils joined together (Figure 3A). The long axe of the spheroids varies from 33 to 220 nm. The lateral dimension of the protofibrils ranges from 17 to 44 nm. The height of the oligomers and protofibrils in a scope of 1 × 1 μm^2 is in the range of 2−19 nm with the maximum distribution at 16 nm (Figure 3C). Small aggregates were also found emerging out of the Aβ_{1-42} sample, which are likely to grow into spheroids or merge into protofibrils.

In contrast, protofibrils were not observed in the sample of Aβ_{1-42} incubated with DC-AB1. However, sparsely distributed Aβ_{1-42} oligomers with a diameter of 4−15 nm were observed (Figure 3B). A statistical analysis in a scope of 3 × 3 μm^2 showed that the height of the oligomers ranges from 1.5 to 2.0 nm with the maximum distribution at 1.8 nm (Figure 3D). Comparing the morphology of the oligomers and protofibrils shown in Figure 3A and B, we can see that DC-AB1 dramatically suppressed the aggregation of Aβ_{1-42}, not only by reducing the size of formed oligomers but also by decreasing the number of nuclei for aggregation, which are critical for fibril formation (*53*). The inhibition of the formation of Aβ protofibrils is consistent with the inhibitory activity of DC-AB1 determined by the ThT fluorescence assay (Figure 2).

Effect of DC-AB1 on Aβ Oligomerization. Glutaraldehyde is a homobifunctional amine cross-linker frequently used for the detection of protein oligomerization (*54*, *55*). We cross-linked Aβ_{1-42} oligomers with glutaraldehyde so that Aβ_{1-42} oligomerization in the presence and absence of DC-AB1 could be studied by polyacrylamide gel electrophoresis analysis. First, we analyzed the uncross-linked Aβ_{1-42} samples on a native gel (Figure 4A). The unincubated Aβ_{1-42} displayed a dark band corresponding to the monomer, whereas the incubated Aβ_{1-42} did not show any band on the gel. Aβ_{1-42} incubated with DC-AB1 displayed a smearing band, indicating the existence of aggregation from monomer to higher ordered multimers. To determine the molecular weight of the oligomers, we analyzed the cross-linked and uncross-linked Aβ_{1-42} samples on SDS−PAGE (Figure 4B). Consistent with the native gel analysis result, the uncross-linked Aβ_{1-42} without incubation showed a dark band corresponding to the Aβ_{1-42} monomer. The incubated Aβ_{1-42} samples, both in the presence and absence of DC-AB1, showed a monomer band on SDS−PAGE. The density of the monomer bands descended in the order of unincubated Aβ_{1-42}, Aβ_{1-42} incubated with DC-AB1, and Aβ_{1-42} incubated without DC-AB1. The Aβ_{1-42} samples cross-linked with glutaraldehyde only displayed monomer bands on SDS−PAGE.

Effect of DC-AB1 on the Conformation of Aβ. Aβ adopts a conformation mixture of α-helix, β-sheet, and random coil in aqueous solution. It undergoes a conformational transition to form intramolecular β-sheet structure in fibrils. However, the conformational transition pathway is still unclear. To

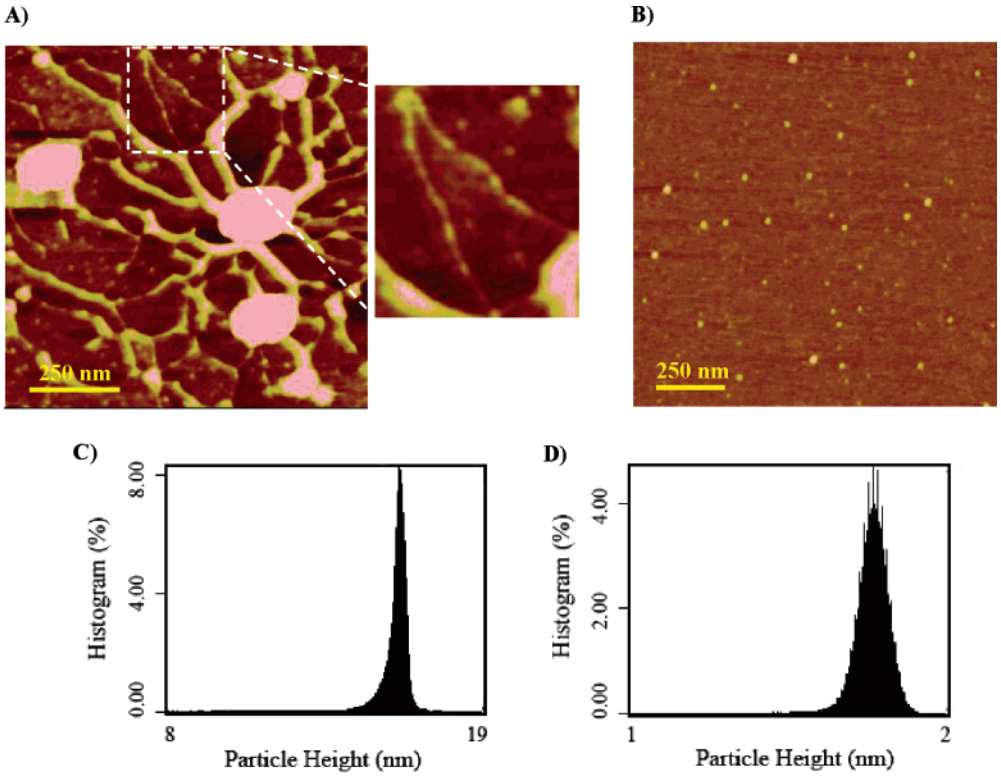

FIGURE 3: Morphological study of Aβ oligomers and fibrils by AFM experiment. (A) $A\beta_{1-42}$ (10 μM) forms protofibrils after 6 days of incubation at 37 °C in 20% TFE. (B) AFM scan image of a 10 μM $A\beta_{1-42}$ peptide sample incubated with 500 μM DC-AB1. (C) Statistical analysis of the particle height of oligomers and protofibrils in an $A\beta_{1-42}$ sample incubated without DC-AB1. (D) Statistical analysis of the particle height of aggregation species in an $A\beta_{1-42}$ sample incubated with DC-AB1.

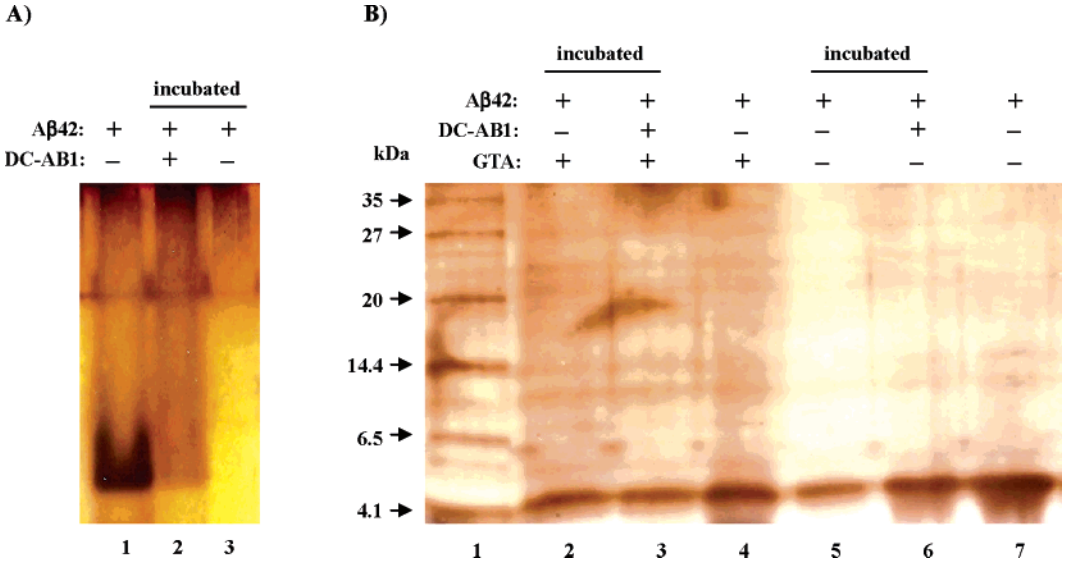

FIGURE 4: Native gel (10%) and 10% SDS−PAGE analysis of $A\beta_{1-42}$ incubated with or without DC-AB1. Equal amounts of $A\beta_{1-42}$ were loaded onto all of the lanes. The gels were run in a Tris/Glycine system and developed by the silver-stain method. (A) Native gel analysis of uncross-linked $A\beta_{1-42}$ samples. Lane 1: unincubated $A\beta_{1-42}$; lane 2: $A\beta_{1-42}$ incubated with DC-AB1; and lane 3: $A\beta_{1-42}$ incubated without DC-AB1. (B) SDS−PAGE analysis of cross-linked and uncross-linked $A\beta_{1-42}$ samples. $A\beta_{1-42}$ were cross-linked with 42 mM glutaraldehyde at room temperature for 20 min. Lane 1: marker; lane 2: cross-linked $A\beta_{1-42}$, incubated without DC-AB1; lane 3: cross-linked $A\beta_{1-42}$, incubated with DC-AB1; lane 4: cross-linked $A\beta_{1-42}$, unincubated; lane 5: uncross-linked $A\beta_{1-42}$, incubated without DC-AB1; lane 6: uncross-linked $A\beta_{1-42}$, incubated with DC-AB1; and lane 7: uncross-linked $A\beta_{1-42}$, unincubated.

investigate how DC-AB1 would affect Aβ aggregation, we studied the conformational change of Aβ induced by the compound with CD spectroscopy (Figure 5). In 20% TFE, a low polar solvent that can stabilize the α-helix and disrupt the interstrand hydrogen bond of β-sheet, $A\beta_{1-40}$ was converted into the α-helical conformation characterized by the negative bands near 208 nm, 220 nm, and the positive band near 193 nm. Interestingly, the addition of DC-AB1 to the $A\beta_{1-40}$ aqueous solution with 20% TFE induced a significant conformational change. The typical negative

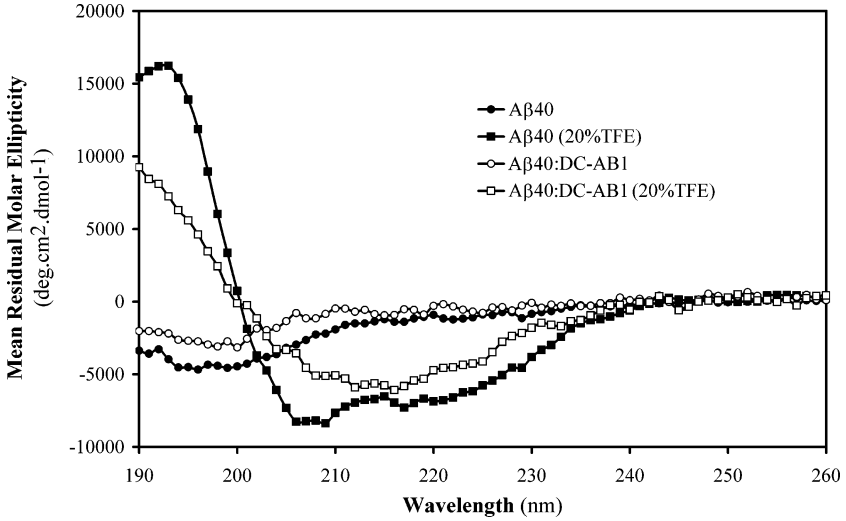

FIGURE 5: CD spectroscopy of Aβ_{1-40} with DC-AB1. The CD spectra were recorded in a 0.1 cm path-length cuvette over a wavelength of 190−260 nm with a scan speed of 100 nm/s at room temperature. The data were the average of four time scans with an interval of 1 nm. The background signal from water was subtracted.

bands at 218 and 220 nm of the α-helix diminished and a negative band at 216 nm was observed, indicating the appearance of the *β*-sheet conformation.

According to the CD deconvolution result (Table 1), Aβ_{1-40} has a conformation mixture containing 5.8% α-helix, 37.0% *β*-sheet, 20.1% *β*-turn, and 35.7% random coil in aqueous solution. In 20% TFE, the content of helical conformation increased from 5.8% to 19.9%, whereas the *β*-sheet conformation decreased from 37.0% to 29.0%, demonstrating the helix stabilization effect of the TFE solvent. When DC-AB1 was added to the 20% TFE solution, the *β*-sheet component increased from 29.0% to 35.8%, and the helical component decreased from 19.9% to 12.5%. The variation of the content of *β*-turn and random coil conformation was relatively small, suggesting that some of the A*β* residues with α-helical conformation had reverted to the *β*-sheet conformation upon interaction with DC-AB1. However, the *β*-sheet content of Aβ_{1-40} after the addition of DC-AB1 is still less than that in aqueous solution because of the helix stabilization effect of the TFE solvent. Likewise, the presence of DC-AB1 in the aqueous solution of Aβ_{1-40} also increased the *β*-sheet content from 37.0% to 43.2% but did not change the helical component. The amount of *β*-turn and random coil conformations decreased from 20.1% to 18.4% and 35.7% to 33.1%, respectively, suggesting that some residues within the *β*-turn and/or random coil regions had been converted into the *β*-sheet conformation.

Table 1: Deconvolution Results of Aβ_{1-40} CD Spectra

	Aβ_{1-40}	(Aβ_{1-40}/ DC-AB1)[a]	Aβ_{1-40} (in 20% TFE)	(Aβ_{1-40}/ DC-AB1)[a] (in 20% TFE)
helix	5.8	5.8	19.9	12.5
β-sheet[b]	37.0	43.2	29.0	35.8
β-turn	20.1	18.4	19.5	19.0
random coil	35.7	33.1	31.2	33.6

[a] Aβ_{1-40} and DC-AB1 are in equimolar concentration. [b] The content of antiparallel *β*-sheet and parallel *β*-sheet conformations.

DISCUSSION

Rationale for the Strategy for Inhibitor Design. The solution structures of Aβ_{1-40} and Aβ_{1-42} have been determined in TFE (*23*), sodium dodecyl sulfate (SDS) micelles (*26*), or HFIP (*21*) by NMR techniques. Both peptides are folded into two helical domains connected by a flexible kink region. The lengths and positions of the helixes are different among these structures, implying that A*β* structures are highly flexible and depend on the solvent properties. Therefore, the resolved NMR structures could not be used directly for the inhibitor design because the buffers used in the NMR experiments are different from the physiological conditions. Besides, A*β* peptides undergo a conformation transition in fibrillogenesis. It is even more difficult to determine the A*β* intermediate structures on the conformational transition pathway by experimental approaches. To explore the structural features of A*β* peptide, we studied the conformational transition of Aβ_{1-40} by using a series of long time molecular dynamics simulations and demonstrated that helix/*β*-sheet mixed conformations are possible intermediates in A*β* fibrillogenesis (*46*). The MD simulations indicated that there were α-helical and *β*-sheet regions on the intermediate structures, suggesting that either the α-helix and/or the *β*-sheet might be targeted for inhibitor design, even though the overall structures of A*β* are flexible.

Meanwhile, MD simulations also revealed that the structural segment of residues 24−40 may be the core domain for A*β* oligomerization and that four glycine residues, Gly-25, Gly-29, Gly-33 and Gly-37, are essential for *β*-sheet formation (*46*). The mutation of the glycine residues with alanine destabilized the *β*-sheet conformation and increased the propensity for an α-helical conformation of this region. Consistent with our MD simulations, a synthesized Aβ_{1-40} peptide analogue with the incorporation of 2-hydroxy-4-methoxybenzyl (Hmb) at 20, 25, 29, 33, and 37 positions to protect the backbone amide did not form fibrils (*56*). In addition, two amino acid elongations (Ile-41 and Ala-42) at the *C*-terminus of Aβ_{1-42} dramatically increases the tendency of aggregation than that in Aβ_{1-40}, which further implies the importance of *C*-terminal residues for A*β* fibril formation. For these reasons, we took the *C*-terminal region of A*β* intermediate structures as the binding site for inhibitor design. Indeed, by using a virtual screening approach, we discovered one small molecule, DC-AB1, that can potently inhibit the A*β* fibril formation.

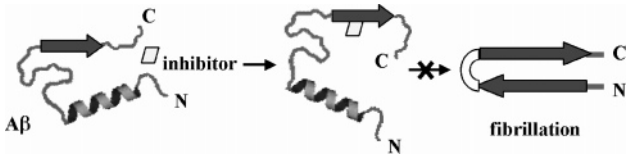

FIGURE 6: Schematic representation of a mechanism for DC-AB1 inhibition of Aβ fibrillation.

Inhibition Mechanism of DC-AB1 to Aβ Fibrillation. According to the complex model of DC-AB1 with $A\beta_{1-40}$ generated by docking simulation, DC-AB1 binds to the *C*-terminal region mainly through hydrophobic interactions (Figure 1B and C). There are three major hydrophobic sites at the $A\beta_{1-40}$ peptide surface that hold the hydrophobic chemical groups of DC-AB1. Two phenyl rings of DC-AB1 interact with the hydrophobic sites constituted of the residues of Val24, Gly29, Val40, or the residues of Tyr10, Phe19, Phe20. The morpholine group of DC-AB1 interacts with the hydrophobic residues of Leu34 and Val40. These interactions are in agreement with previously published experimental results. It has been reported that a pentapeptide incorporating the sequence of $A\beta_{16-20}$, KLVFF, can prevent the assembly of Aβ into fibrils (*57*). Three mutants at Lys16, Leu17, and Phe20 with alanine markedly reduced Aβ fibrillation capability, suggesting that this sequence is critically involved in Aβ fibrillation. The hydrophobic interaction of the phenyl ring of DC-AB1 with Tyr10, Phe19, and Phe20 interfered with the crucial role of the sequence KLVFF in Aβ fibrillation. This may be one of the reasons that DC-AB1 showed Aβ fibrillation inhibiting activity. Meanwhile, a tetrapeptide, Pr−IIGLa, can self-aggregate into β-pleated sheet structure; however, another pentapeptide, RIIGLa, derived from $A\beta_{30-34}$, which shares the sequence of IIGL with Pr-IIGLa, was able to inhibit Aβ fibrillization (*58*), suggesting the importance of the four residues IIGL in fibril formation. Therefore, the interaction of the morpholine group of DC-AB1 with residues Leu34 and Val40 may constitute another reason for the inhibitory activity of DC-AB1 against Aβ fibrillation. The consistency of the interaction between Aβ residues and DC-AB1 with experimental results support the rationality of our inhibitor design strategy.

The conformational change of Aβ induced by DC-AB1 was studied by CD spectroscopy. As shown in Figure 5 and Table 1, the binding of DC-AB1 increased the β-sheet content of Aβ peptide. There are two possible mechanisms that could explain the increasing amount of β-sheet conformation. The binding of DC-AB1 at the *C*-terminal region of the intermediate structure, as discussed above, might stabilize or promote β-sheet conformation of the monomeric peptide. However, we are not able to exclude another possibility that DC-AB1 could induce intermolecular β-sheet formation of Aβ through the hydrophobic interaction between the *C*-terminal regions, which might explain the formation of small spherical $A\beta_{1-42}$ oligomers when incubated with DC-AB1 (Figure 3B).

On the basis of the docking simulation and experimental results, we propose a mechanism for DC-AB1 inhibition of Aβ fibrillation as depicted in Figure 6. DC-AB1 binds to the *C*-terminal region of Aβ intermediates on the conformational transition pathway mainly through hydrophobic interactions. The interaction between DC-AB1 and the *C*-terminal region shields the key residues at the *C*-terminus from interacting with the residues at the *N*-terminus, thereby interrupting Aβ to form antiparallel β-sheet structure that is a rate-determining step toward fibril formation (*59*). Consequently, it inhibited Aβ fibrillation.

Implications for the Mechanism of Aβ Fibrillation. Different from the contact-mode AFM in which the investigated objects are often pushed away by the stylus during scanning, the stylus in tapping-mode AFM touches the objects only at the end of its downward movement. The contact time and friction forces that might distort the morphology of the fibrils are reduced. Therefore, the tapping-mode AFM is more suitable for the study of the morphology of amyloid fibrils. After 6 days of incubation at 37 °C, $A\beta_{1-42}$ at 10 μM in 20% TFE formed spheroidic oligomers and branched protofibrils of 2−19 nm height with the maximum distribution at 16 nm. The protofibrils are about 17−44 nm in width, indicating that $A\beta_{1-42}$ formed ribbon-like protofibrils. Amyloid fibrils are usually in the shape of straight cylinders of 6−10 nm diameter; however, the environment can affect the morphology of the fibrils into twisted ropes, tubes, or ribbons (*60*). The ribbon-like branched protofibrils of $A\beta_{1-42}$ formed at 10 μM in 20% TFE are different from the typical cylindrical amyloid fibrils, suggesting that the fibrillation pathway of $A\beta_{1-42}$ in 20% TFE is not identical to the one through which amyloid peptides formed into straight cylindrical fibrils. In the presence of DC-AB1, $A\beta_{1-42}$ formed sparsely distributed oligomers with a height of 1.5−2.0 nm and a diameter of 4−15 nm, indicating a flat spherical shape of the oligomers. No protofibrils were observed. The morphological study of Aβ peptide by AFM clearly proved the inhibitory activity of the compound.

As to the fibrillogenesis of amyloid peptides, several models have been proposed, one of which is the critical oligomers model (*61*). According to this model, the first step in fibrillogenesis is the formation of critical oligomers, which is followed by coalescence of the critical oligomers into protofibrils. The inhibition mechanism of DC-AB1 and its effects on the ultrastructure (Figure 3), oligomerization (Figure 4), and conformation (Figure 5) of Aβ imply that the intermediate states with an α-helix/β-sheet mixture structure indeed exist during the conformational transition of Aβ. The residues at the β-sheet region of the *C*-terminus would interact with the *N*-terminal residues to form antiparallel β-sheet structures, which may aggregate into oligomers. Consistent with this hypothesis, numerous spheroidic species of different sizes were emerging out of the $A\beta_{1-42}$ incubation sample as shown in Figure 3A. The close up, framed out by the dashed rectangle in Figure 3A, shows that the oligomers lined up and coalesced with each other to merge into protofibrils. The assembly of the oligomers vividly showed the development from small spherical structures to protofibrils. Meanwhile, $A\beta_{1-42}$ can also aggregate into 60-kDa globulomers through a pathway independent of the fibril formation (*62*). The *C*-terminus residues 24−42 of $A\beta_{1-42}$ formed the core of the globulomer with the *N*-terminus hydrophilic residues 1−19 or 1−23 exposed at the outer surface, making the globulomer highly water soluble. The globulomers bind specifically to hippocampal neurons and have been detected in amyloid plaques in the brains of AD patients. Our AFM experiment demonstrated that in addition to the formation of protofibrils, $A\beta_{1-42}$ also formed 33−220 nm spheroidic

oligomers that are much wider than amyloid fibrils (Figure 3A). It is possible that these big spheroidic oligomers could be globulomers or even higher ordered oligomers, which is worthy of further study because the coexistence of protofibrils and globulomers in Aβ fibrillogenesis may help us understand the formation of amyloid plaques in the brains of AD patients.

We further studied Aβ oligomerization in the presence or absence of DC-AB1 by using native gel and SDS−PAGE. The dissociation of Aβ oligomers and fibrils by SDS is well-known (*63*). However, it is also reported that SDS can induce the oligomerization of Aβ peptide (*54*). To stabilize Aβ oligomers and fibrils for SDS−PAGE analysis, we used glutaraldehyde to cross-link Aβ samples. Equal amounts of Aβ_{1-42} were loaded onto the lanes for all of the analyzed Aβ_{1-42} samples. On the native gel, Aβ_{1-42} from stock solution without incubation adopts a monomeric form (Figure 4A, lane 1). After 6 days of incubation, the monomer band disappeared, suggesting that Aβ_{1-42} had aggregated into higher ordered oligomers and fibrils (Figure 4A, lane 3). The fibrillation of Aβ_{1-42} had been inhibited by DC-AB1, demonstrated by the smearing band of the monomer to multimers on the native gel (Figure 4A, lane 2). On SDS−PAGE, a monomer band was observed on the lanes for three uncross-linked Aβ_{1-42} samples. The appearance of the monomer band for incubated Aβ_{1-42} sample on SDS−PAGE indicated that Aβ oligomers or fibrils had been disassembled into monomers by SDS (Figure 4B, lane 5). Also, Aβ_{1-42} multimers formed in the presence of DC-AB1 as shown on the native gel were disassembled into monomers by SDS (Figure 4B, lane 6). No oligomer bands were observed for all three uncross-linked Aβ_{1-42} samples. Considering that glutaraldehyde could stabilize the oligomers, we cross-linked Aβ_{1-42} samples with 42 mM GTA. However, Aβ oligomers were still not observed (Figure 4B, lanes 2, 3, and 4). There may be two reasons that explain the invisibility of oligomer bands on SDS−PAGE. The first reason is that a trace amount of oligomers formed in 30 μM Aβ_{1-42} might not be enough for detection by the silver-stain method. In addition to increasing the Aβ_{1-42} concentration, similar to what another group did using $\geq$100 μM Aβ for an oligomerization study by SDS−PAGE (*27*), more sensitive detection methods such as Western-blot should perform better than the silver-stain method. Besides, even with cross-linking by glutaraldehyde, no oligomers bands appeared on SDS−PAGE, suggesting that a more efficient cross-linking method such as photoinduced cross-linking of unmodified proteins (PICUP) is required (*64*−*67*). Another reason for the invisibility of oligomers bands on SDS−PAGE is related to the dissociation of Aβ oligomers and/or fibrils by SDS. It should be noted that not all of the Aβ oligomeric forms and/or fibrils had been disassembled by SDS. An important conclusion could be drawn by comparing the density of the monomer bands of Aβ_{1-42} incubated without DC-AB1 and unincubated Aβ_{1-42} on SDS−PAGE. Though the loading amount of Aβ_{1-42} was the same for both lanes, the density of the monomer band from Aβ_{1-42} incubated without DC-AB1 (Figure 4B, lane 5) is lighter than the density of the monomer band from unincubated Aβ_{1-42} (Figure 4B, lane 7), indicating that incubated Aβ_{1-42} had formed into SDS-resistant oligomers and/or fibrils. This conclusion is in line with the previous report of SDS-stable Aβ oligomers extracted from Chinese hamster ovary (CHO) cells expressing β-amyloid protein precursor genes (*68*).

A variety of computational methods for library screening, *de novo* design, evaluation of drug-likeness, and protein−ligand binding affinity have been developed for drug design and discovery (*69*). Structure-based drug design techniques that require the 3D structure information of drug targets have been proven successful in bringing about 40 compounds into clinical trials and numerous others to drug approvals (*70*). When the structural information of drug targets is unavailable, some techniques such as pharmacophore map or QSAR model could be used for drug design. However, it is still a challenge to design small molecules that interrupt the protein−protein interaction, especially for unknown structural or nonstructural targets. To our knowledge, the small inhibitor of Aβ that we presented here is the first example of drug design targeting nonstructured peptides. As explained above, Aβ peptides adopt a conformation mixture of random coil, α-helix, and β-sheet in aqueous solution with the tendency to aggregation and fibrillization. Apparently, the conformation mixture of Aβ and the conformational change toward fibrils make it extraordinarily difficult to design new Aβ inhibitors because Aβ are basically nonstructural, and we do not know which intermediate conformation could be the effective target for the design. To circumvent this problem, we employed molecular dynamics simulations to study the conformational transition of Aβ and determined the *C*-terminal β-sheet region as the target for inhibitor design. By using virtual screening in conjunction with fluorescence bioassays and AFM experiments, we discovered a new small molecule that binds Aβ and inhibits fibrillation. The study not only demonstrated a drug design strategy targeting nonstructured proteins but also validated the fact that the *C*-terminal β-sheet region of Aβ intermediate structures could be used as a binding site for Aβ inhibitor design. The discovery of the inhibitor also indirectly proved the existence of the α-helix/β-sheet intermediates during Aβ fibrillation as predicted by our previous MD simulations, which may help understand the aggregation mechanism of Aβ in Alzheimer's disease.

ACKNOWLEDGMENT

We thank Professor Irwin D. Kuntz for providing the source code for DOCK4.0.

SUPPORTING INFORMATION AVAILABLE

HPLC analysis and high-resolution mass spectral data of the identified compound. This material is available free of charge via the Internet at http://pubs.acs.org.

REFERENCES

1. Geula, C., Wu, C. K., Saroff, D., Lorenzo, A., Yuan, M., and Yankner, B. A. (1998) Aging renders the brain vulnerable to amyloid beta-protein neurotoxicity, *Nat. Med. 4*, 827−831.
2. Glenner, G. G., and Wong, C. W. (1984) Alzheimer's disease: initial report of the purification and characterization of a novel cerebrovascular amyloid protein, *Biochem. Biophys. Res. Commun. 120*, 885−890.
3. Selkoe, D. J. (1994) Alzheimer's disease: a central role for amyloid, *J. Neuropathol. Exp. Neurol. 53*, 438−447.
4. Iwatsubo, T., Odaka, A., Suzuki, N., Mizusawa, H., Nukina, N., and Ihara, Y. (1994) Visualization of A beta 42(43) and A beta 40 in senile plaques with end-specific A beta monoclonals:

evidence that an initially deposited species is A beta 42(43), *Neuron 13*, 45−53.
5. Suzuki, N., Cheung, T. T., Cai, X. D., Odaka, A., Otvos, L. J., Eckman, C., Golde, T. E., and Younkin, S. G. (1994) An increased percentage of long amyloid beta protein secreted by familial amyloid beta protein precursor (beta APP717) mutants, *Science 264*, 1336−1340.
6. Dahlgren, K. N., Manelli, A. M., Stine, W. B. J., Baker, L. K., Krafft, G. A., and LaDu, M. J. (2002) Oligomeric and fibrillar species of amyloid-beta peptides differentially affect neuronal viability, *J. Biol. Chem. 277*, 32046−32053.
7. Selkoe, D. J. (1999) Translating cell biology into therapeutic advances in Alzheimer's disease, *Nature 399*, A23−A31.
8. Kagan, B. L., Hirakura, Y., Azimov, R., Azimova, R., and Lin, M. C. (2002) The channel hypothesis of Alzheimer's disease: current status, *Peptides 23*, 1311−1315.
9. Monji, A., Utsumi, H., Ueda, T., Imoto, T., Yoshida, I., Hashioka, S., Tashiro, K., and Tashiro, N. (2001) The relationship between the aggregational state of the amyloid-beta peptides and free radical generation by the peptides, *J. Neurochem. 77*, 1425−1432.
10. Sultana, R., Newman, S., Mohmmad-Abdul, H., Keller, J. N., and Butterfield, D. A. (2004) Protective effect of the xanthate, D609, on Alzheimer's amyloid beta-peptide (1−42)-induced oxidative stress in primary neuronal cells, *Free Radical Res. 38*, 449−458.
11. Tabner, B. J., El-Agnaf, O. M., Turnbull, S., German, M. J., Paleologou, K. E., Hayashi, Y., Cooper, L. J., Fullwood, N. J., and Allsop, D. (2005) Hydrogen peroxide is generated during the very early stages of aggregation of the amyloid peptides implicated in Alzheimer disease and familial British dementia, *J. Biol. Chem. 280*, 35789−35792.
12. Holtzman, D. M. (2004) In vivo effects of ApoE and clusterin on amyloid-beta metabolism and neuropathology, *J. Mol. Neurosci. 23*, 247−254.
13. Lauderback, C. M., Kanski, J., Hackett, J. M., Maeda, N., Kindy, M. S., and Butterfield, D. A. (2002) Apolipoprotein E modulates Alzheimer's Abeta(1−42)-induced oxidative damage to synaptosomes in an allele-specific manner, *Brain Res. 924*, 90−97.
14. Sadowski, M., Pankiewicz, J., Scholtzova, H., Ripellino, J. A., Li, Y., Schmidt, S. D., Mathews, P. M., Fryer, J. D., Holtzman, D. M., Sigurdsson, E. M., and Wisniewski, T. (2004) A synthetic peptide blocking the apolipoprotein E/beta-amyloid binding mitigates beta-amyloid toxicity and fibril formation in vitro and reduces beta-amyloid plaques in transgenic mice. *Am. J. Pathol. 165*, 937−948.
15. Lustbader, J. W., Cirilli, M., Lin, C., Xu, H. W., Takuma, K., Wang, N., Caspersen, C., Chen, X., Pollak, S., Chaney, M., Trinchese, F., Liu, S., Gunn-Moore, F., Lue, L. F., Walker, D. G., Kuppusamy, P., Zewier, Z. L., Arancio, O., Stern, D., Yan, S. S., and Wu, H. (2004) ABAD directly links Abeta to mitochondrial toxicity in Alzheimer's disease, *Science 304*, 448−452.
16. Oppermann, U. C., Salim, S., Tjernberg, L. O., Terenius, L., and Jornvall, H. (1999) Binding of amyloid beta-peptide to mitochondrial hydroxyacyl-CoA dehydrogenase (ERAB): regulation of an SDR enzyme activity with implications for apoptosis in Alzheimer's disease, *FEBS Lett. 451*, 238−242.
17. Klein, W. L., Krafft, G. A., and Finch, C. E. (2001) Targeting small Abeta oligomers: the solution to an Alzheimer's disease conundrum? *Trends Neurosci. 24*, 219−224.
18. Lansbury, P. T., Jr. (1997) Inhibition of amyloid formation: a strategy to delay the onset of Alzheimer's disease, *Curr. Opin. Chem. Biol. 1*, 260−267.
19. Danielsson, J., Jarvet, J., Damberg, P., and Graslund, A. (2005) The Alzheimer beta-peptide shows temperature-dependent transitions between left-handed 3-helix, beta-strand and random coil secondary structures, *FEBS J. 272*, 3938−3949.
20. Zhang, S., Iwata, K., Lachenmann, M. J., Peng, J. W., Li, S., Stimson, E. R., Lu, Y., Felix, A. M., Maggio, J. E., and Lee, J. P. (2000) The Alzheimer's peptide a beta adopts a collapsed coil structure in water, *J. Struct. Biol. 130*, 130−141.
21. Crescenzi, O., Tomaselli, S., Guerrini, R., Salvadori, S., D'Ursi, A. M., Temussi, P. A., and Picone, D. (2002) Solution structure of the Alzheimer amyloid beta-peptide (1−42) in an apolar microenvironment. Similarity with a virus fusion domain, *Eur. J. Biochem. 269*, 5642−5648.
22. Fezoui, Y., and Teplow, D. B. (2002) Kinetic studies of amyloid beta-protein fibril assembly. Differential effects of alpha-helix stabilization, *J. Biol. Chem. 277*, 36948−36954.
23. Sticht, H., Bayer, P., Willbold, D., Dames, S., Hilbich, C., Beyreuther, K., Frank, R. W., and Rosch, P. (1995) Structure of amyloid A4-(1−40)-peptide of Alzheimer's disease, *Eur. J. Biochem. 233*, 293−298.
24. Vieira, E. P., Hermel, H., and Mohwald, H. (2003) Change and stabilization of the amyloid-beta(1−40) secondary structure by fluorocompounds, *Biochim. Biophys. Acta 1645*, 6−14.
25. Barrow, C. J., Yasuda, A., Kenny, P. T., and Zagorski, M. G. (1992) Solution conformations and aggregational properties of synthetic amyloid beta-peptides of Alzheimer's disease. Analysis of circular dichroism spectra, *J. Mol. Biol. 225*, 1075−1093.
26. Coles, M., Bicknell, W., Watson, A. A., Fairlie, D. P., and Craik, D. J. (1998) Solution structure of amyloid beta-peptide(1−40) in a water-micelle environment. Is the membrane-spanning domain where we think it is? *Biochemistry 37*, 11064−11077.
27. Stine, W. B. J., Dahlgren, K. N., Krafft, G. A., and LaDu, M. J. (2003) In vitro characterization of conditions for amyloid-beta peptide oligomerization and fibrillogenesis, *J. Biol. Chem. 278*, 11612−11622.
28. Kirschner, D. A., Abraham, C., and Selkoe, D. J. (1986) X-ray diffraction from intraneuronal paired helical filaments and extraneuronal amyloid fibers in Alzheimer disease indicates cross-beta conformation, *Proc. Natl. Acad. Sci. U.S.A. 83*, 2776.
29. Ippel, J. H., Olofsson, A., Schleucher, J., Lundgren, E., and Wijmenga, S. S. (2002) Probing solvent accessibility of amyloid fibrils by solution NMR spectroscopy, *Proc. Natl. Acad. Sci. U.S.A. 99*, 8648−8653.
30. Luhrs, T., Ritter, C., Adrian, M., Riek-Loher, D., Bohrmann, B., Dobeli, H., Schubert, D., and Riek, R. (2005) 3D structure of Alzheimer's amyloid-beta(1−42) fibrils. *Proc. Natl. Acad. Sci. U.S.A. 102*, 17342−17347.
31. Kirkitadze, M. D., Condron, M. M., and Teplow, D. B. (2001) Identification and characterization of key kinetic intermediates in amyloid beta-protein fibrillogenesis, *J. Mol. Biol. 312*, 1103−1119.
32. Mandal, P. K., and Pettegrew, J. W. (2004) Alzheimer's disease: soluble oligomeric Abeta(1−40) peptide in membrane mimic environment from solution NMR and circular dichroism studies, *Neurochem. Res. 29*, 2267−2272.
33. Walsh, D. M., Hartley, D. M., Kusumoto, Y., Fezoui, Y., Condron, M. M., Lomakin, A., Benedek, G. B., Selkoe, D. J., and Teplow, D. B. (1999) Amyloid beta-protein fibrillogenesis. Structure and biological activity of protofibrillar intermediates, *J. Biol. Chem. 274*, 25945−25952.
34. Howlett, D. R., George, A. R., Owen, D. E., Ward, R. V., and Markwell, R. E. (1999) Common structural features determine the effectiveness of carvedilol, daunomycin and rolitetracycline as inhibitors of Alzheimer beta-amyloid fibril formation, *Biochem. J. 343*, 419−423.
35. Howlett, D. R., Perry, A. E., Godfrey, F., Swatton, J. E., Jennings, K. H., Spitzfaden, C., Wadsworth, H., Wood, S. J., and Markwell, R. E. (1999) Inhibition of fibril formation in beta-amyloid peptide by a novel series of benzofurans, *Biochem. J. 340*, 283−289.
36. Abe, K., Kato, M., and Saito, H. (1997) Congo red reverses amyloid beta protein-induced cellular stress in astrocytes, *Neurosci. Res. 29*, 129−134.
37. Lee, V. M. (2002) Amyloid binding ligands as Alzheimer's disease therapies, *Neurobiol. Aging 23*, 1039−1042.
38. Zhuang, Z. P., Kung, M. P., Hou, C., Skovronsky, D. M., Gur, T. L., Plössl, K., Trojanowski, J. Q., Lee, V. M., and Kung, H. F. (2001) Radioiodinated styrylbenzenes and thioflavins as probes for amyloid aggregates, *J. Med. Chem. 44*, 1905−1914.
39. Kim, H., Park, B. S., Lee, K. G., Choi, C. Y., Jang, S. S., Kim, Y. H., and Lee, S. E. (2005) Effects of naturally occurring compounds on fibril formation and oxidative stress of beta-amyloid, *J. Agric. Food Chem. 53*, 8537−8341.
40. Gordon, D. J., Sciarretta, K. L., and Meredith, S. C. (2001) Inhibition of beta-amyloid(40) fibrillogenesis and disassembly of beta-amyloid(40) fibrils by short beta-amyloid congeners containing *N*-methyl amino acids at alternate residues, *Biochemistry 40*, 8237−8245.
41. Kisilevsky, R., Szarek, W., and Weaver, D. (1999) Method for treating amyloidosis, U.S. Patent 5,972,328.
42. Cherny, R. A., Atwood, C. S., Xilinas, M. E., Gray, D. N., Jones, W. D., McLean, C. A., Barnham, K. J., Volitakis, I., Fraser, F. W., Kim, Y., Huang, X., Goldstein, L. E., Moir, R. D., Lim, J. T., Beyreuther, K., Zheng, H., Tanzi, R. E., Masters, C. L., and Bush, A. I. (2001) Treatment with a copper−zinc chelator

markedly and rapidly inhibits beta-amyloid accumulation in Alzheimer's disease transgenic mice, *Neuron 30*, 665−676.
43. Dominguez, D. I., and De Strooper, B. (2002) Novel therapeutic strategies provide the real test for the amyloid hypothesis of Alzheimer's disease, *Trends Pharmacol. Sci. 23*, 324−330.
44. Helmuth, L. (2000) An antibiotic to treat Alzheimer's? *Science 290*, 1273−1274.
45. Tabira, T. (2001) Clioquinol's return: cautions from Japan. *Science 292*, 2251−2252.
46. Xu, Y., Shen, J., Luo, X., Zhu, W., Chen, K., Ma, J., and Jiang, H. (2005) Conformational transition of amyloid beta-peptide, *Proc. Natl. Acad. Sci. U.S.A. 102*, 5403−5407.
47. Ewing, T. J. A., and Kuntz, I. D. (1997) Critical evaluation of search algorithms for automated molecular docking and database screening, *J. Comput. Chem. 18*, 1175−11789.
48. Kuntz, I. D. (1992) Structure-based strategies for drug design and discovery, *Science 257*, 1078−1082.
49. Clark, R. D., Strizhev, A., Leonard, J. M., Blake, J. F., and Matthew, J. B. (2002) Consensus scoring for ligand/protein interactions, *J. Mol. Graphics Modell. 20*, 281−295.
50. Lee, K. H., Shin, B. H., Shin, K. J., Kim, D. J., and Yu, J. (2005) A hybrid molecule that prohibits amyloid fibrils and alleviates neuronal toxicity induced by beta-amyloid(1−42), *Biochem. Biophys. Res. Commun. 328*, 816−823.
51. Bohm, G., Murh, R., and Jaenicke, R. (1992) Quantitative analysis of protein far UV circular dichroism spectra by neural networks, *Protein Eng. 5*, 191−195.
52. LeVine, H., III. (1993) Thioflavine T interaction with synthetic Alzheimer's disease beta-amyloid peptides: detection of amyloid aggregation in solution, *Protein Sci. 2*, 404−410.
53. Lomakin, A., Teplow, D. B., Kirschner, D. A., and Benedek, G. B. (1997) Kinetic theory of fibrillogenesis of amyloid beta-protein, *Proc. Natl. Acad. Sci. U.S.A. 94*, 7942−7947.
54. LeVine, H., III. (1995) Soluble multimeric Alzheimer beta(1−40) pre-amyloid complexes in dilute solution, *Neurobiol. Aging 16*, 755−764.
55. Quist, A., Doudevski, I., Lin, H., Azimova, R., Ng, D., Frangione, B., Kagan, B., Ghiso, J., and Lal, R. (2005) Amyloid ion channels: a common structural link for protein-misfolding disease, *Proc. Natl. Acad. Sci. U.S.A. 102*, 10427−10432.
56. Clippingdale, A. B., Macris, M., Wade, J. D., and Barrow, C. J. (1999) Synthesis and secondary structural studies of penta(acetyl-Hmb)A beta(1−40), *J. Pept. Res. 53*, 665−672.
57. Tjernberg, L. O., Naslund, J., Lindqvist, F., Johansson, J., Karlstrom, A. R., Thyberg, J., Terenius, L., and Nordstedt, C. (1996) Arrest of beta-amyloid fibril formation by a pentapeptide ligand, *J. Biol. Chem. 12*, 15.
58. Fulop, L., Zarandi, M., Datki, Z., Soos, K., and Penke, B. (2004) Beta-amyloid-derived pentapeptide RIIGLa inhibits Abeta(1−42) aggregation and toxicity, *Biochem. Biophys. Res. Commun. 324*, 64−69.
59. Petty, S. A., and Decatur, S. M. (2005) Intersheet rearrangement of polypeptides during nucleation of {beta}-sheet aggregates, *Proc. Natl. Acad. Sci. U.S.A. 1753*, 108−120.
60. Stromer, T., and Serpell, L. C. (2005) Structure and morphology of the Alzheimer's amyloid fibril, *Microsc. Res. Tech. 67*, 210−217.
61. Modler, A. J., Gast, K., Lutsch, G., and Damaschun, G. (2003) Assembly of amyloid protofibrils via critical oligomers—a novel pathway of amyloid formation, *J. Mol. Biol. 325*, 135−148.
62. Barghorn, S., Nimmrich, V., Striebinger, A., Krantz, C., Keller, P., Janson, B., Bahr, M., Schmidt, M., Bitner, R. S., Harlan, J., Barlow, E., Ebert, U., and Hillen, H. (2005) Globular amyloid beta-peptide oligomer: a homogeneous and stable neuropathological protein in Alzheimer's disease, *J. Neurochem. 95*, 834−847.
63. Walsh, D. M., Lomakin, A., Benedek, G. B., Condron, M. M., and Teplow, D. B. (1997) Amyloid beta-protein fibrillogenesis. Detection of a protofibrillar intermediate, *J. Biol. Chem. 272*, 22364−22372.
64. LeVine, H., III. (2004) Alzheimer's beta-peptide oligomer formation at physiologic concentrations. *Anal. Biochem. 335*, 81−90.
65. Bitan, G., Lomakin, A., and Teplow, D. B. (2001) Amyloid beta-protein oligomerization: prenucleation interactions revealed by photo-induced cross-linking of unmodified proteins, *J. Biol. Chem. 276*, 35176−35184.
66. Bitan, G., Kirkitadze, M. D., Lomakin, A., Vollers, S. S., Benedek, G. B., and Teplow, D. B. (2003) Amyloid beta -protein (Abeta) assembly: Abeta 40 and Abeta 42 oligomerize through distinct pathways. *Proc. Natl. Acad. Sci. U.S.A. 100*, 330−335.
67. Bitan, G., and Teplow, D. B. (2004) Rapid photochemical cross-linking—a new tool for studies of metastable, amyloidogenic protein assemblies, *Acc. Chem. Res. 37*, 357−364.
68. Podlisny, M. B., Ostaszewski, B. L., Squazzo, S. L., Koo, E. H., Rydell, R. E., Teplow, D. B., and Selkoe, D. J. (1995) Aggregation of secreted amyloid beta-protein into sodium dodecyl sulfate-stable oligomers in cell culture, *J. Biol. Chem. 270*, 9564−9670.
69. Jorgensen, W. L. (2004) The many roles of computation in drug discovery, *Science 303*, 1813−1818.
70. Congreve, M., Murray, C. W., and Blundell, T. L. (2005) Structural biology and drug discovery, *Drug Discovery Today 10*, 895−907.

BI060955F